PAPER

Channel Modeling and Performance Analysis of Diversity Reception for Implant UWB Wireless Link

Jingjing SHI[†a)], ***Student Member***, **Daisuke ANZAI**[†b)], ***Member***, ***and*** **Jianqing WANG**[†c)], ***Fellow***

SUMMARY This paper aims at channel modeling and bit error rate (BER) performance improvement with diversity reception for in-body to on-body ultra wideband (UWB) communication for capsule endoscope application. The channel characteristics are firstly extracted from 3.4 to 4.8 GHz by using finite difference time domain (FDTD) simulations incorporated with an anatomical human body model, and then a two-path impulse response channel model is proposed. Based on the two-path channel model, a spatial diversity reception technique is applied to improve the communication performance. Since the received signal power at each receiver location follows a lognormal distribution after summing the two path components, we investigate two methods to approximate the lognormal sum distribution in the combined diversity channel. As a result, the method matching a short Gauss-Hermite approximation of the moment generating function (MGF) of the lognormal sum with that of a lognormal distribution exhibits high accuracy and flexibility. With the derived probability density function (PDF) for the combined diversity signals, the average BER performances for impulse-radio (IR) UWB with non-coherent detection are investigated to clarify the diversity effect by both theoretical analysis and computer simulation. The results realize an improvement around 10 dB on Eb/No at BER of 10^{-3} for two-branch diversity reception.

key words: *ultra-wideband (UWB), in-body to on-body communication, channel model, spatial diversity, bit error rate (BER)*

1. Introduction

A wireless body area network (WBAN) is composed of a small scale network inside, on or in the proximity of a human body. WBANs can be divided into wearable BANs and implant BANs. In modern society, it is expected to be one of the main technologies that can provide extremely high convenience and high efficiency in assisting healthcare or medical services [1]. For example, a capsule endoscope is a typical implant BAN application in which an in-body to on-body wireless link is required. The capsule endoscope may be swallowed as a pill by a patient and implement examinations by taking photographs or videos and then transmit them to the outside receiver especially for the small intestine where is difficult to make diagnoses and treat without performing operations. Such a medical application requires a reliable wireless communication channel, high data rate for real-time transmission, and extremely low power consumption for increasing device longevity. The application of UWB technology offers a possibility for this wireless link to fulfill the above requirements [2]. However, on the basis of recent researches on UWB propagation in human body [3], [4], it is clear that the in-body transmission has to be limited to the low-band, for example, from 3.4 to 4.8 GHz as defined in Japan. This is because that the higher transmitting frequency is, the smaller penetration depth of human tissues is.

Owing to the complex properties of human tissues, transmitted low-band UWB signals still suffer from large attenuation and shadowing which may lead to undesired performance degradation for the in-body to on-body wireless link. A diversity reception technique has been adopted for improving the quality and reliability in UWB wireless BAN [5], [6]. In order to employ a diversity reception technique, it is of great importance to establish an appropriate channel model for the in-body to on-body transmission. Many past efforts focus on on-body or in-body to off-body channels [7]–[10]. Despite there are few works have been made to clarify the channel characteristics for implant BAN [4], [11], there is no investigation of the channel characteristics for spatial diversity reception. The spatial diversity channel characteristics are thus derived from this study.

This study aims at the channel modeling and diversity analysis for in-body to on-body UWB wireless link for a capsule endoscope. The channel model is firstly established based on the finite difference time domain (FDTD) numerical simulations incorporated with an anatomical human body model. Then the probability density function (PDF) of combined diversity channel is derived by using two approximation methods and their accuracy is compared. Finally the diversity effect is investigated by both theoretical analysis and computer simulation for impulse radio UWB (IR-UWB) with non-coherent detection over the in-body to on-body shadowing channel. This work contributes to not only the practical design of capsule endoscope application, but also other healthcare applications for implant BAN with low-band UWB techniques.

2. Analysis Model

The analysis model of human body with antennas on its surface to receive the capsule endoscope data is illustrated in Fig. 1. The human body model is constituted of detailed anatomical structure which has nearly 50 types of tissue and 2-mm spatial resolution [12]. The transmitting antenna of the capsule endoscope was assumed as a 4-mm long dipole moving in the small intestine to take 33 locations. It also had

Manuscript received November 25, 2011.
Manuscript revised April 25, 2012.

[†]The authors are with the Graduate School of Engineering, Nagoya Institute of Technology, Nagoya-shi, 466-8555 Japan.
a) E-mail: chx17507@stn.nitech.ac.jp
b) E-mail: anzai@nitech.ac.jp
c) E-mail: wang@nitech.ac.jp

DOI: 10.1587/transcom.E95.B.3197

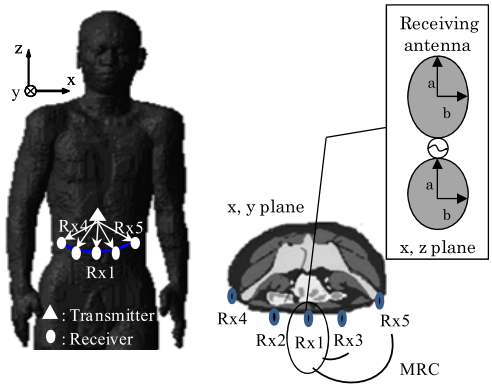

Fig. 1 FDTD analysis model with spatial diversity reception for capsule endoscope.

polarization directions x, y, and z based on practical moving rotations of capsule endoscope. The transmitted UWB signal is a Gaussian-pulse-modulated sine signal with a width of 2.1 ns, in which most of the energy can be captured between 3.4 and 4.8 GHz. On the other hand, on account of the consideration of spatial diversity in this case, as shown in Fig. 1 the receiving antenna was arranged at five receiver locations in front of the abdomen for spatial diversity reception. The five receivers were located at one cross section, in x-y plane. Rx1 is in the centre of abdomen, Rx2 and Rx4 are on the left side of Rx1, Rx3 and Rx5 are on the right side of Rx1. The receivers were located with a spacing of 2 mm from the body surface, and the distance between each two receiver locations was about 6.5 cm. The receiving antennas were designed to have an elliptic disc structure, as described in [10] in detail. They had the specification of a=7 cm in major radius axis and b=5 cm in minor radius axis, respectively, and were arranged to have a z-directed polarization. The standing wave ratio (VSWR) of the elliptic disc dipole antennas was almost flat, and lower than 2 from 3.4 to 4.8 GHz at UWB low band. As a result, in each on-body receiver location, we obtained 99 data for extracting the propagation channel characteristics. Therefore, by using such a simulation model, we can not only derive the propagation channel characteristics of each single communication branch, but also can evaluate the spatial diversity effect of any two or more than two combined branches. Moreover, since the propagation channel characterizations were made by using FDTD numerical method incorporated with an anatomical human body model, we applied one-relaxation Debye approximation to represent frequency-dependent human tissue properties. It has been revealed in [13] that the maximum difference between one-relaxation Debye approximation and measured dielectric property data is less than 10% in UWB low band.

3. Channel Modeling

In order to realize a reliable in-body to on-body communication, it is important to know the in-body to on-body channel characteristics and to establish an appropriate channel model. Based on the established channel model, we can determine adequate receiver structure and improve communication performance.

3.1 Impulse Response Model

The UWB signal arriving at each receiver location through the in-body to on-body channel is a sum of several attenuated, delayed and eventually distorted replicas of the transmitted signal. A discrete time impulse response approximation model for characterizing the in-body to on-body channel may be used and can be expressed by modifying the popular Saleh-Valenzuela model appropriately as [14]

$$h(t) = \sum_{k=1}^{N} \alpha_k \delta(t - \tau_k) \tag{1}$$

where α_k is the multipath gain coefficient, τ_k is the delay of the arrival time of the k-th multipath component relative to the first path, and N is the total number of the multipath components. Relative to the impulse response, power delay profile (PDP) is a statistical description for a multipath channel, and can be obtained from the temporal average of $h(\tau) \cdot h^*(\tau)$. The time axis in the impulse response or PDP can be divided into small intervals named bins and the bin width is usually the same as time resolution.

Here from the FDTD simulations, we obtained 99 impulse responses at each receiver location for the in-body to on-body channel in total. The FDTD-simulated impulse response was calculated from

$$h(t) = F^{-1}\left[H(f)\right] = F^{-1}\left[\frac{U_r(f)}{U_s(f)}\right] \tag{2}$$

where $U_r(f)$ and $U_s(f)$ are received and transmitted pulse energies, respectively. $H(f)$ is the frequency domain transfer function, and F^{-1} [] indicates the inverse Fourier transform. During the process of inverse Fourier transform, the Hamming window with a coefficient of 2 was applied in the frequency domain in order to limit the transmitted pulse signal to effective frequency components. Therefore, the time resolution of $h(t)$ in Eq. (1) was approximated as the Hamming window coefficient multiplied by the reciprocal of the additional window function bandwidth, resulting in a 1.43 ns time resolution. In other words, multipath components within such a time width cannot be resolved even if more than one multipath arrives. Due to this limited time resolution, we divided the time axis into many bins where each bin has a width of 1.43 ns. So in each impulse response or PDP, the first multipath was identified from the first peak of bins, and the second and the third multipath components were identified from the successive bins respectively.

Figure 2 shows a typical FDTD-derived PDP for the in-body to on-body multipath channel. In this case, the receiving antenna was located in front of human abdomen as Rx1, while the transmitting antenna was from one of the 33 locations with one polarization. The first multipath component can be considered as a direct path between the transceiver

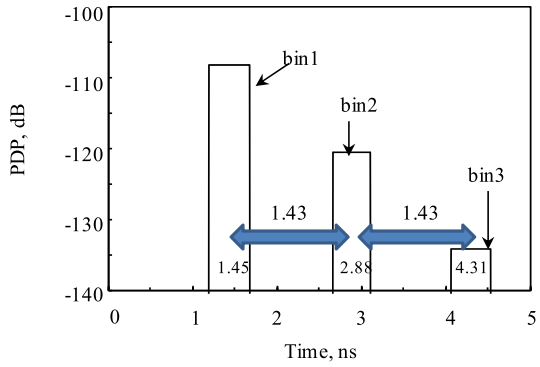

Fig. 2 Typical FDTD-derived power delay profile for in-body to on-body channel. Transmitter location is 10.6 cm away from Rx1 with z polarization. The values of 1.45 ns, 2.88 ns, and 4.31 ns indicate the arrival time of the first, second, and third bins of multipath components, respectively.

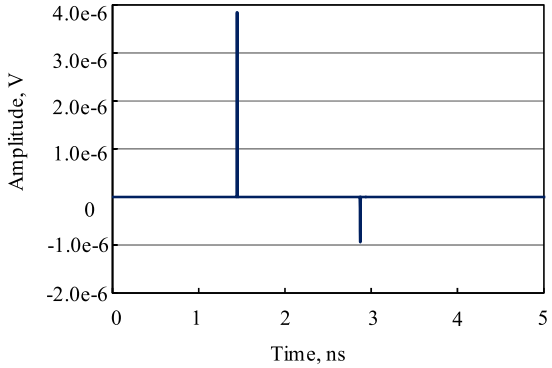

Fig. 3 Example of approximated two-path impulse response model.

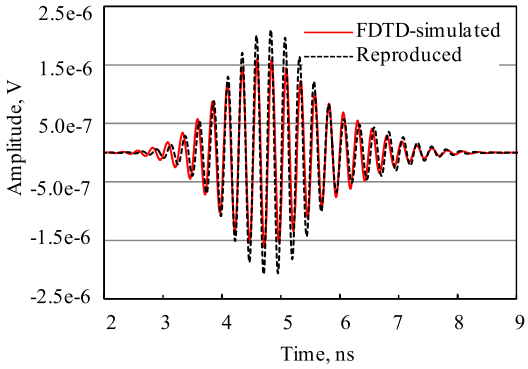

Fig. 4 Waveform comparison between reproduced and FDTD-simulated results.

and receiver and its arrival time was identified from the first peak of multipath components as 1.45 ns. As a consequence, the successive multipath components can be assumed to correspond to the components diffracted by or scattering from various organs and tissues of the human body. In fact, there should be a lot of multipath components occurred inside human body because it does have a very complicated structure. Due to the limited time resolution of 1.43 ns in this study, however, we cannot separate all multipath components correctly for various organs and tissues. Although the multipath components cannot be fully resolved, we can consider the multipath components within the second or third bin as a summarization of various diffracted or scattered components within that time width. We thus identified the arrival time of the second multipath component as 2.88 ns by adding the bin width (1.43 ns) to the first multipath component's arrival time (1.45 ns). Similarly, we also identified the third multipath component and the following ones by the same method. Moreover, the arrival time of the first multipath component can also be estimated by calculating the division of in-body to on-body local distance (10.6 cm) and the propagation speed in human body (about a quarter of light speed in free space). The resulting result of about 1.45 ns provides a good agreement with the first multipath component observed in Fig. 2.

In addition, also from other results of the derived impulse responses or PDPs for different transmitting and receiving pairs, the direct path always turned out to be the strongest path with comparison to the successive multipath components. Since the power of the multipath component from the third bin was more than 25 dB lower than the first one, which was weak enough to be neglected, the first two multipath components with a fixed bin width were taken in account as dominating multipath components. Therefore, we proposed an approximation of discrete time impulse response channel model with only two multipath components, the first multipath component corresponds to direct path, and the second one corresponds to a dominating diffracted or scattered path, which also means the total multipath components number N in Eq. (1) is 2.

Figure 3 shows an example of approximated two-path impulse response model at the receiver location Rx1. The amplitude of this two-path impulse model was calculated from the integrated power within one bin in the corresponding PDP, and the time interval between these two paths was assumed to be as same as one bin width. In order to validate whether this proposed two-path model is appropriate or not, we conducted a reproduction of the received pulse waveform by applying the convolution, where the transmitted pulse is convoluted by the approximated two-path model. The reproduced pulse can be expressed as

$$v_r(t) = v_s(t) \otimes h(t) \tag{3}$$

where $v_r(t)$ denotes the reproduced pulse, $v_s(t)$ and $h(t)$ are the transmitted pulse and approximated two-path impulse response, respectively. Comparison of the reproduced received pulse and FDTD-simulated received pulse is shown in Fig. 4. As can be seen, the reproduced pulse reaches a good agreement with the FDTD-simulated pulse, and the correlation coefficient between them was found to be as high as 0.92. Moreover, the other occasions for different pairs of transmitting and receiving locations have also been confirmed to have a high correlation coefficient around 0.9 when a two-path impulse response model was adopted. As a result, it can be concluded that a two-path impulse response model is sufficient to produce an appropriate approximation to the received pulse signals. It also suggests that in-body to

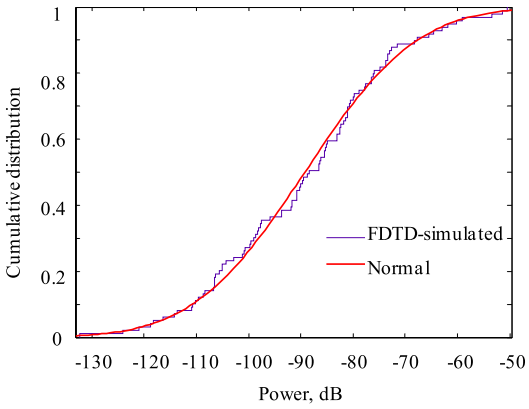

Fig. 5 Cumulative distribution of 1st path power. Since the power is expressed in decibel, the fitting result is normal distribution.

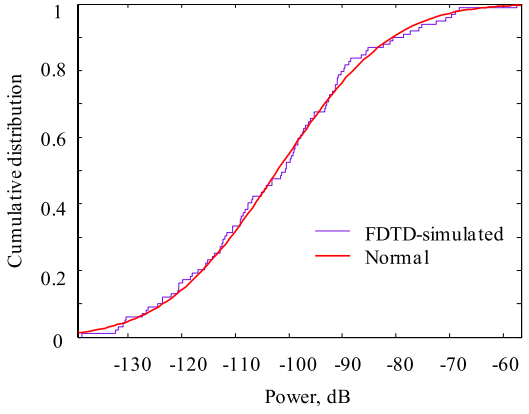

Fig. 6 Cumulative distribution of 2nd path power. Since the power is expressed in decibel, the fitting result is normal distribution.

on-body channel characteristics mainly depend on the large attenuation with less influence of multipath.

Based on such a well approximated two-path model, the multipath power distributions were investigated to provide the parameters in view of statistical respect. Here the multipath powers for the two paths were fitted to some candidate statistical distributions, respectively. As shown in Fig. 5 and Fig. 6, the normal distribution provides a superior fit to both of the two-path magnitudes in decibel based on the second-order Akaike Information Criterion [7]. That is to say, the lognormal distribution fits well the two-path powers. The average standard deviations of the power variation were found to be 16.8 dB. At the same time, a difference of less than 15 dB between the two multipath components was found when the cumulative density function (CDF) was 0.5.

The arrival time of the first multipath component from the in-body to on-body transmission is significantly determined by the direct path transmission, but varies at different transmitting locations and polarizations. The information on arrival time of the first path is essential for diversity reception. From FDTD-simulated results, 99 different arrival times of direct path were obtained at each receiver location. It was found that the inverse Gaussian distribution fits well the derived arrival times of direct path also based on the second-order Akaike Criterion. The mean μ and the standard deviation σ of the inverse Gaussian distribution were found to be 1.3 ns and 0.54 ns. Moreover, since the inter-path delay corresponding to the temporal delay between two successive multipath components was assumed as a fixed bin width (1.43 ns) in this study, the second path had the same statistical distribution but a longer mean arrival time of 2.73 ns. Based on the above characterization, the parameters of the two-path impulse response model are summarized in Table 1 for the UWB in-body to on-body wireless link.

Table 1 Main parameters for in-body to on-body UWB impulse response channel model.

Description		Characteristics	Parameters
1st path	Power	Lognormal	$\mu_1 = -89.2dB$ $\sigma_1 = 16.8dB$
	Arrival time	Inverse Gaussian	$\mu_1 = 1.3ns$ $\lambda_1 = 7.5ns$
2nd path	Power	Lognormal	$\mu_2 = -102.3dB$ $\sigma_2 = 16.8dB$
	Arrival time	Inverse Gaussian	$\mu_2 = 2.73ns$ $\lambda_2 = 7.5ns$

3.2 Path Loss Model

In view of the two-path channel model, we can at first capture the maximum power of each single branch and identify it as the direct path. Then the second path would be recognized consequently from the arrival time of the direct path plus the fixed bin width. Thus, the received signals can be added up with the adoption of a two-finger RAKE reception [10]. However, it may be not easy to separate the two paths with such a small time interval as 1.43 ns in actual receiver realization. Instead of RAKE reception, for a pulse position modulation (PPM) or on-off keying (OOK) scheme in IR-UWB, the first and second path contributions can be summed by integrating the received signals within the first two bins and then demodulated with an envelope or energy detector. Therefore, even if we cannot separate the delayed signal correctly due to the limited time resolution, the received signal can still be appropriately captured with the aid of channel model parameters. So it is also useful to get a path loss model based on the received signal energy.

By using the analysis model in Sect. 2, we obtained the instant FDTD-calculated path loss for each single communication channel in decibel. It should be noticed that the calculated path loss contains the effects of the transmitting and receiving antennas because of the difficulty in correctly removing them in such a near-field situation. The path loss model can be expressed as a distance-dependent equation include the shadowing, given by an empirical power decay law function as

$$PL_{dB} = PL_{0,dB} + 10n \log_{10} \frac{d}{d_0} + S_{dB} \quad (4)$$

where d is the distance from the in-body transmitting an-

Table 2 Parameters of path loss model at each receiving location.

Rx location	$PL_{0,dB}$	n	$S(\mu,\sigma)$
Rx1	48.6	10.6	(1,1.88)
Rx2	46.7	12.6	(1,1.95)
Rx3	48.5	8.0	(1,1.76)
Rx4	52.4	6.2	(1,1.80)
Rx5	44.5	12.8	(1,1.63)

Table 3 Correlation coefficients between each two combining channels.

	Rx1	Rx2	Rx3	Rx4	Rx5
Rx1	1.0				
Rx2	0.10	1.0			
Rx3	0.24	0.34	1.0		
Rx4	0.13	0.52	0.28	1.0	
Rx5	0.18	0.44	0.49	0.51	1.0

tenna to the on-body receiving antenna, d_0 is the reference distance (0.05 m), $PL_{0,dB}$ is the path loss at the reference distance, n is the path loss exponent, and S_{dB} is called as shadowing which is caused by different organs surrounding the transmitter and fluctuates around the average path loss. Table 2 gives the parameters fitted by using the least-squares method, which provides a good fit to the FDTD-calculated path loss of the in-body to on-body channel. In addition, the statistical distribution of the shadowing in decibel S_{dB} was found to be well approximated by normal distribution. That is to say, the lognormal distribution fits well our in-body to on-body shadowing data S at each receiver location. The parameters μ and σ of the lognormal distributed shadowing at each receiving location are also summarized in Table 2.

Moreover, the correlation coefficients between the received signals at different receiver locations were also calculated to confirm the possibility of spatial diversity. The correlation coefficient of each two single channels can be obtained from

$$\rho = \frac{\sum_{m=1}^{M}\left(U_{ri,m}-\overline{U_{ri}}\right)\left(U_{rj,m}-\overline{U_{rj}}\right)}{\sqrt{\sum_{m=1}^{M}\left(U_{ri,m}-\overline{U_{ri}}\right)^2\sum_{i=1}^{M}\left(U_{rj,m}-\overline{U_{rj}}\right)^2}} \tag{5}$$

where M=99 is data number corresponding to different transmitter locations, $U_{ri,m}$ and $U_{rj,m}$ are instant FDTD-calculated received energies at any two receiver locations among Rx1, Rx2, Rx3, Rx4, Rx5, and $\overline{U_{ri}}$, $\overline{U_{rj}}$ indicate their average values, respectively. Table 3 gives the calculated correlation coefficients for all of the combinations of the five receiver locations. In order to realize a significant diversity effect, the received signals at different locations should have smaller correlation. As can be seen, the correlation coefficient ranges from 0.1 to 0.5, which suggests the feasibility of spatial diversity.

Although the channel characteristics were derived only from one human body model, the model has been developed with a sufficient consideration and adjustment to have average mass and dimensions of Japanese male for various organs and tissues. So the derived channel parameters should have sufficient generality, i.e., described average channel characteristics. Of course some deviations in the channel parameters may exist between different human body models. To clarify this point is considered as a future subject.

4. MRC Diversity Reception

The diversity reception refers to a method for improving the reliability of a signal by combining two or more communication channels with different characteristics. This can be achieved by using two or more receivers, which is known as spatial diversity reception. Our analysis model shown in Fig. 1 may accord with this placement requirement. The combining method considered here is maximum ratio combining (MRC) in terms of spatial diversity. It represents a theoretically optimal combiner compared to other diversity schemes in which the desired signal-to-noise power ratio (SNR) can be maximized over fading channels in a communication system.

Based on the in-body to on-body channel characteristics derived in previous section, the combined signal with MRC diversity over two lognormal distributed channels can be denoted as a lognormal sum distribution. The derivation of this lognormal sum PDF is therefore of great importance for evaluating the average BER on this in-body to on-body wireless link.

The average BER performance after MRC diversity reception over an in-body to on-body transmission can be given by

$$P_{MRC}(\overline{\gamma}) = \int_0^\infty p_0(\gamma)\, p(\gamma) d\gamma \tag{6}$$

where γ indicates E_b/N_0 (energy per bit to noise power spectral density ratio), $p_0(\gamma)$ indicates bit error probability of the received signal assumed to be corrupted by additive white Gaussian noise (AWGN) for IR-UWB with PPM or OOK modulation scheme, $p(\gamma)$ indicates lognormal sum PDF.

4.1 Lognormal Sum PDF

Given the importance of the lognormal sum distribution in analyzing this in-body to on-body wireless system performance, efforts have been devoted to derive the PDF of lognormal sum distribution. However, any general exact closed-form theoretical expressions for lognormal sum PDF are unknown. As opposed to this, several approximation methods have been proposed in which the lognormal sum can still be approximated as a lognormal distribution. Subsequently, we attempted to employ two different approximation methods, named A and B here, to derive the corresponding parameters for the approximating lognormal sum PDF.

Method A is referred from [15] which gives a very simple and straightforward formula to approximate the parameters μ and σ from individual μ_1, σ_1 and μ_2, σ_2 in separate lognormal distributions as shown in the following equation

$$\mu = \mu_1 + \mu_2,$$

$$\sigma = k\sqrt{\sigma_1^2 + \sigma_2^2} \tag{7}$$

where k is a correction coefficient to adjust the approximated σ. It is given by

$$k = 1 - 0.5(D_1 - D_2)^2 \tag{8}$$

where D_1 and D_2 are the standard deviations of the two lognormal distributions, respectively. This approximation formula has been validated by Monte Carlo simulation to have a reasonable accuracy.

In comparison with Method A, Method B is a more analytical and flexible approximation method which is to match a short Gauss-Hermite approximation of the moment generating function (MGF) of the lognormal sum with that of a lognormal distribution, as proposed in [16]. The parameters μ and σ in decibel in the lognormal sum PDF were suggested to be solved from the following equation

$$\begin{aligned}\sum_{n=1}^{N} \frac{w_n}{\sqrt{\pi}} \exp\left[-s_m \exp\left(\frac{\sqrt{2}\sigma_{dB}a_n + \mu_{dB}}{\xi}\right)\right] \\ = \sum_{n=1}^{N} \frac{w_n}{\sqrt{\pi}} \exp\left[-s_m \exp\left(\frac{\sqrt{2}\sigma_{1,dB}a_n + \mu_{1,dB}}{\xi}\right)\right] \\ \times \sum_{n=1}^{N} \frac{w_n}{\sqrt{\pi}} \exp\left[-s_m \exp\left(\frac{\sqrt{2}\sigma_{2,dB}a_n + \mu_{2,dB}}{\xi}\right)\right], \\ \text{for m=1 and 2.}\end{aligned} \tag{9}$$

In Eq. (9), $\xi = 10\log_e 10$ is a scaling constant. The weights w_i and abscissas a_n for the Gauss-Hermite series expansion are tabulated in [17]. The Hermite integration order N is suggested as 6. s_m indicates the parameter for adjusting the weighted integrals of the short Gauss-Hermit integration, whose value can be chosen flexibly. It therefore plays an important role for contributing to an accurate lognormal sum approximation. In this study we determined it as a typical value $(s_1, s_2) = (0.1, 1.5)$ based on the fitting accuracy to the FDTD-derived PDF curve. It was found that lognormal sum PDFs of any two channels' combination from Rx1 to Rx5 can provide a good approximation with these s_1 and s_2 values. So these s_1 and s_2 values are suitable to any two combined in-body to on-body channels for capsule endoscope application. The non-linear equations with unknown parameters of μ and σ in decibel in the left term of Eq. (9) were numerically solved using fsolve function in Matlab. For simplicity, the in-body to on-body lognormal fading channel at each receiving location was assumed to be independent spatially.

Figure 7 shows the PDF based on FDTD-derived data and the PDFs approximated by the two different lognormal sum approximation methods versus normalized receiving power. There are two situations investigated in this study. One as shown in Fig. 7(a) is for the MRC diversity of Rx1 and Rx3, and the other one as shown in Fig. 7(b) is for MRC diversity of Rx1 and Rx5. The approximated parameters in the lognormal sum for MRC diversity using methods A and B are given in Table 4. As can be seen from Fig. 7, the

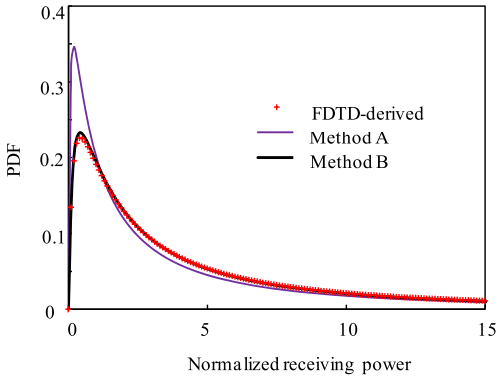

(a) PDFs for MRC of Rx1 and Rx3.

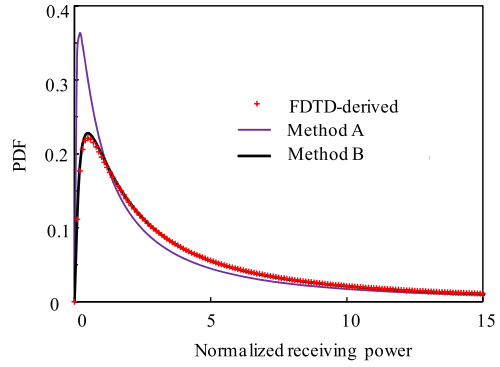

(b) PDFs for MRC of Rx1 and Rx5.

Fig. 7 Derived PDFs based on FDTD-simulated data using approximation methods A and B.

Table 4 Lognormal parameter for MRC channel.

MRC	Method A (μ,σ)	Method B (μ,σ)
Rx1&Rx3	(1.06,1.61)	(1.21,1.44)
Rx1&Rx5	(1.02,1.58)	(1.19,1.38)

Method B gave a better approximation to the FDTD-derived PDF compared with Method A, especially for the maximum of the PDF. In order to quantitatively compare the accuracy of the two approximation results with the FDTD-derived result, we calculated the correlation between them and found that the correlation coefficients were 0.99 for Method B but 0.95 or 0.93 for Method A. Although Method B needs to solve a non-linear equation, it gives a higher accuracy in deriving the lognormal sum PDF. We therefore determined to use the derived lognormal sum PDF with Method B in the average BER analysis. In addition, compared with the results in Table 2, we observed that the parameter σ for MRC diversity becomes smaller than that for single branch no matter which approximation method we adopt.

4.2 Average BER Performance

A theoretical analysis on BER performance contributes to a quantitative evaluation for the communication performance

over the in-body to on-body wireless link. Incorporating with the IR-UWB technology in which an extremely short pulse is transmitted with no carrier frequency, a typical modulation scheme known as PPM or OOK was considered to derive the BER performance. With PPM scheme, the information of the data bit to be transmitted was encoded by the position of the transmitted UWB pulse with respect to a nominal position, the received data was then go through a non-coherent envelope detector to obtain the reproduction of the transmitted data. On the other hand, the IR-UWB with OOK scheme is also attractive because of its simple structure. The BER performance for both PPM and OOK were therefore theoretically derived.

By using the lognormal sum PDF $p(\gamma)$ with approximated parameters in Table 4 and the bit error probability for PPM or OOK in AWGN channel with non-coherent detection [18], we calculated the average BER for MRC diversity of Rx1 and Rx3, and MRC diversity of Rx1 and Rx5, respectively. Figures 8 and 9 depict the average BER performances of the two branch MRC diversity. Also the BER under AWGN channel was plotted in these two figures, and the average BER without MRC were plotted on the right side of the figures at each single branch Rx1 and Rx3, respectively. The graphically plotted BER performance versus E_b/N_0 of PPM is in Fig. 8, and that of OOK is in Fig. 9.

In order to clarify the validity of the theoretical approximation by using Method B as well as the diversity effect, computer simulations were also conducted under the same condition as the theoretical analysis. The simulated BER results were plotted in these figures with symbols. The good accordance between the theoretically approximated BER and computer simulated BER was observed not only in a single branch but also in the MRC diversity reception. Obvious BER improvements were obtained at least 9 dB for both PPM and OOK at BER of 10^{-3}, and the diversity gain of 2 was achieved. The derived results with OOK as shown in Fig. 9 were about 3 dB degraded in comparison with that of PPM. That is because with the same data rate and noise power in these two considered schemes, the bandwidth per bit with PPM is twice of that with OOK, which contributes to a half noise power spectral density to PPM.

From Figs. 8 and 9, Method B has been shown to be sufficiently effective as an approximation method to the lognormal sum PDF in in-body to on-body MRC diversity channels. Moreover, it should also be noted that Method B provides a very high parametric flexibility which can handle the inaccuracy problem in different regions for the approximation of the lognormal sum PDF.

In addition, combining Rx1 and Rx5 with MRC diversity has also been confirmed to have the same tendency with that of Rx1 and Rx3. Since the combined signal after MRC diversity for Rx1 and Rx5 has a smaller σ compared to that for Rx1 and Rx3 in Table 4, a somewhat better average BER performance improvement is observed up to 12 dB based on theoretical approximation with Method B at BER of 10^{-3}. In total, a smaller σ value in the approximated lognormal PDF for the MRC diversity may yield a better BER performance.

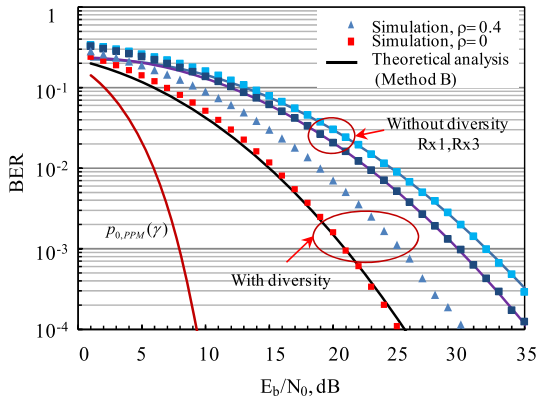

Fig. 8 Average BER performance with PPM scheme for diversity of Rx1 and Rx3. Results indicated by solid lines are based on theoretical analysis. Results indicated by symbols are based on computer simulation. ρ denotes correlation coefficient.

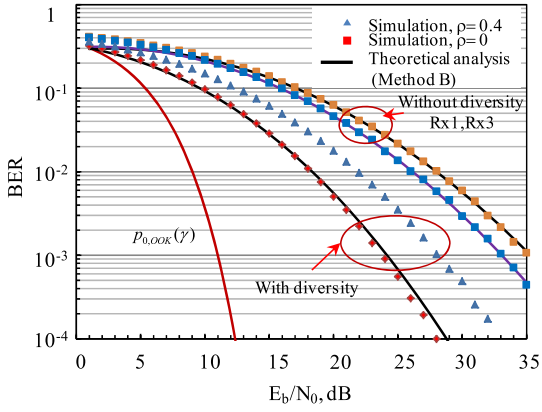

Fig. 9 Average BER performance with OOK scheme for diversity of Rx1 and Rx3. Results indicated by solid lines are based on theoretical analysis. Results indicated by symbols are based on computer simulation. ρ denotes correlation coefficient.

Similarly, we obtained the diversity effect by combining any two channels from in-body to on-body in Fig. 1, and the difference between them is not so significant, i.e., smaller than 2 dB. It is therefore possible to choose any two receiver positions in Fig. 1 to obtain a diversity effect around 9–12 dB at BER of 10^{-3}.

However, the theoretical derivation of the lognormal sum distribution assumes statistical independency between two receiving signals. It is not really true because a correlation coefficient between each two single received signals of 0.1–0.5 may exist. Since it is difficult to theoretically derive the PDF of lognormal sum distribution if broke the assumption of independency of each two single channels, we conducted computer simulation to clarify the degree of degradation on the average BER due to the correlation between two receiving signals. The validity of the computer simulation has been confirmed in Figs. 8 and 9. As a result, we found that the higher correlation coefficient is, the larger degradation of the BER performance is. The BER performances with an average correlation coefficient of 0.4 are plotted also in Fig. 8 and Fig. 9. The degradation at BER of 10^{-3} was ob-

served as 4 dB compared to the BER with correlation coefficient of zero. Therefore, the possible diversity improvement would be around 5–8 dB when consider a correlation coefficient of 0.4. Of course if we choose the combination of channels with a smaller correlation coefficient such as 0.1, the diversity improvement will be considerably close to 9–12 dB at BER of 10^{-3}. If we further combine all of the five channels, a diversity effect much larger than 10 dB can be expected.

5. Conclusions

UWB technology in low band has the potential to provide real-time in-body to on-body image transmission for capsule endoscope application, however it suffers from rapid attenuation and shadowing in human tissues. Spatial diversity is an effective mean to cope with this problem. In this study, we firstly analyzed the in-body to on-body propagation characteristics and proposed a two-path impulse response channel model based on the FDTD numerical simulations incorporated with an anatomical human body model. The multipath power and arrival time in the two-path channel model have been clarified as lognormal distribution and inverse Gaussian distribution, respectively. A main feature of the two-path channel model is that the first path is always the strongest and the second path has a fixed time interval from the first path. This feature makes it easy to adopt a non-coherent envelope or energy detection at the receiver.

In view of this feature, we derived a path loss model with shadowing just based on the total received power at each receiver. Since the shadowing in each received low-band UWB signal also follows a lognormal distribution, the lognormal sum distribution for MRC diversity signals has also been approximated as a lognormal distribution. The PDF of combined low-band UWB signal has been derived with two different approximation methods. The method B with MGF has provided a more accurate result with flexible parameters. With the derived lognormal sum PDF, theoretical BER predication of MRC diversity for the in-body to on-body transmission has been performed and its validity has been confirmed by computer simulation. The average BER has shown a diversity effect of around 9–12 dB for PPM and OOK at BER of 10^{-3} with no correlation, 5–8 dB with a correlation coefficient of 0.4, for two branch MRC diversity. These results suggest a significant improvement in the low-band UWB transmission for capsule endoscope application.

The future subject may be the design and realization of actual diversity reception structure.

Acknowledgment

This study was supported in part by Japan Society for the Promotion of Science (No. 21560395).

References

[1] A.W. Astrin, H.-B. Li, and R. Kohno, "Standardization for body area networks," IEICE Trans. Commun., vol.E92-B, no.2, pp.366–372, Feb. 2009.
[2] J. Shi and J. Wang, "Dual-mode impulse radio ultra-wideband transmission for body area networks," IET Microwave Antennas Propagat., vol.5, pp.1250–1255, July 2011.
[3] J. Wang and Q. Wang, "Channel modeling and BER performance of an implant UWB body area link," 2nd Int. Symp. on Applied Sciences in Biomedical and Communication Tech., Bratislava, Slovak, Nov. 2009.
[4] A. Khaleghi, R. Chavez-Santiago, X. Liang, I. Balasingham, V.C.M. Leung, and T. Ramstad, "On ultra wideband channel modeling for in-body communications," Proc. 5th IEEE Int. Symp. on Wireless Pervasive Computing, pp.140–145, Modena, Italy, May 2010.
[5] Y. Chen, J. Teo, J.C.Y. Lai, E. Gunawan, K.S. Low, C.B. Soh, and P.B. Rapajic, "Cooperative communications in ultra-wideband wireless body area networks: Channel modeling and system diversity analysis," IEEE J. Sel. Areas Commun., vol.27, no.1, pp.5–16, Jan. 2009.
[6] J. Shi and J. Wang, "Channel characterization and diversity feasibility for in-body to on-body communication using low-band UWB signals," 3rd Int. Symp. on Applied Sciences in Biomedical and Communication Tech., Rome, Itlay, Nov. 2010.
[7] A. Fort, C. Desset, P. De Doncker, P. Wambacq, and L. Van Biesen, "An ultra-wideband body are propagation channel model: From statistics to implementation," IEEE Trans. Microw. Theory Tech., vol.54, no.4, pp.1820–1826, April 2006.
[8] A. Taparugssanagorn, A. Rabbachin, M. Hamalainen, J. Saloranta, and J. Iinatti, "A review of channel modeling for wireless body area network in wireless medical communications," Proc. 11th Int. Symp. on Wireless Personal Multimedia Communications (WPMC'08), Lapland, Finland, FL3-1, Sept. 2008.
[9] Q. Wang and J. Wang, "Performance of ultra wide band on-body communication based on statistical channel model," IEICE Trans. Commun., vol.E93-B, no.4, pp.833–841, April 2010.
[10] J. Wang, K. Masami, and Q. Wang, "Transmission performance of an in-body to off-body UWB communication link," IEICE Trans. Commun., vol.E94-B, no.1, pp.150–157, Jan. 2011.
[11] S. Matsuda, H. Harada, and R. Kohno, "A study on stochastic radiowave propagation model inside a human body," IEICE Technical Report, WBS2005-59, Dec. 2005.
[12] T. Nagaoka, S. Watanabe, K. Saurai, E. Kunieda, S. Watanabe, M. Taki, and Y. Yamanaka, "Development of realistic high-resolution whole-body voxel models of Japanese adult males and females of average height and weight, and application of models to radio-frequency electromagnetic-field dosimetry," Phys. Med. Biol., vol.49, pp.1–15, 2004.
[13] Q. Wang and J. Wang, "SA and SAR analysis for wearable UWB body area applications," IEICE Trans. Commun., vol.E92-B, no.2, pp.425–430, Feb. 2009.
[14] A.F. Molisch, "Ultra-wide-band propagation channels," Proc. IEEE, vol.97, no.2, pp.353–371, Feb. 2009.
[15] H. Hamaguchi and S. Kanda, "On the distribution of sum of lognormal random variables," Summaries of Technical Papers of Annual Meeting of Architectural Institute of Japan, 2074, Aug. 1992.
[16] J. Wu, N.B. Mehta, and J. Zhang, "A flexible lognormal sum approximation method," Proc. IEEE Globecom 2005, pp.3413–3417.
[17] M. Abramowitz and I. Stegun, Handbook of Mathematical Functions with Formulas, Graphs, and Mathematical Tables, Dover, 9th ed., 1972.
[18] J.C. Bic, D. Duponteil, and J.C. Imbeaus, Elements of Digital Communication, pp.230–234, John Wiley & Sons, 1991.

Jingjing Shi received the B.E. degree in electronic engineering from Shenyang University of Chemical Technology, Shenyang, China, in 2007, and M.E. degree in engineering physics, electronics and mechanics from Nagoya Institute of Technology, Nagoya, Japan, in 2010. From 2008 to 2010, she was engaged in large scale integration circuit design of active noise cancelling system. She is currently at the computer science and engineering department of Nagoya Institute of Technology, working toward her Ph.D. degree. Her research interests include body area communications for healthcare and medical applications especially of in-body to on-body communication.

Daisuke Anzai received the B.E., M.E. and Ph.D. degrees from Osaka City University, Osaka, Japan in 2006, 2008 and 2011, respectively. Since April 2011, he has been an Assistant Professor at the Graduate School of Engineering, Nagoya Institute of Technology, Nagoya, Japan. He has engaged in the research of biomedical communication systems and localization systems in wireless communication networks.

Jianqing Wang received the B.E. degree in electronic engineering from Beijing Institute of Technology, Beijing, China, in 1984, and the M.E. and D.E. degrees in electrical and communication engineering from Tohoku University, Sendai, Japan, in 1988 and 1991, respectively. He was a Research Associate at Tohoku University and a Senior Engineer at Sophia Systems Co., Ltd., prior to joining the Nagoya Institute of Technology, Nagoya, Japan, in 1997, where he is currently a Professor. His research interests include biomedical communications and electromagnetic compatibility.